AFRL-RX-WP-TP-2010-4142

AN INTEGRATED TOOL FOR ESTIMATION OF MATERIAL MODEL PARAMETERS (PREPRINT)

S. Ghosal, N. Acharya, and T.E. Abrahamson

SC Solutions, Inc.

H.W. Schreier

Correlated Solutions, Inc.

APRIL 2010

STINFO COPY

AIR FORCE RESEARCH LABORATORY
MATERIALS AND MANUFACTURING DIRECTORATE
WRIGHT-PATTERSON AIR FORCE BASE, OH 45433-7750
AIR FORCE MATERIEL COMMAND
UNITED STATES AIR FORCE

REPORT DOCUMENTATION PAGE

The public reporting burden for this collection of information is estimated to average 1 hour per response, including the time for reviewing instructions, searching existing data sources, gathering and maintaining the data needed, and completing and reviewing the collection of information. Send comments regarding this burden estimate or any other aspect of this collection of information, including suggestions for reducing this burden, to Department of Defense, Washington Headquarters Services, Directorate for Information Operations and Reports (0704-0188), 1215 Jefferson Davis Highway, Suite 1204, Arlington, VA 22202-4302. Respondents should be aware that notwithstanding any other provision of law, no person shall be subject to any penalty for failing to comply with a collection of information if it does not display a currently valid OMB control number. **PLEASE DO NOT RETURN YOUR FORM TO THE ABOVE ADDRESS**.

1. REPORT DATE *(DD-MM-YY)*	2. REPORT TYPE	3. DATES COVERED *(From - To)*
April 2010	Technical Paper Preprint	01 April 2010 – 01 April 2010

4. TITLE AND SUBTITLE

AN INTEGRATED TOOL FOR ESTIMATION OF MATERIAL MODEL PARAMETERS (PREPRINT)

5a. CONTRACT NUMBER
FA8650-05-C-7251

5b. GRANT NUMBER

5c. PROGRAM ELEMENT NUMBER
65502F

6. AUTHOR(S)

S. Ghosal, N. Acharya, and T.E. Abrahamson (SC Solutions, Inc.)
H.W. Schreier (Correlated Solutions, Inc.)

5d. PROJECT NUMBER
3005

5e. TASK NUMBER
ML

5f. WORK UNIT NUMBER
211T0100

7. PERFORMING ORGANIZATION NAME(S) AND ADDRESS(ES)

SC Solutions, Inc.
1261 Oakmead Parkway
Sunnyvale, CA 94085

Correlated Solutions, Inc.

8. PERFORMING ORGANIZATION REPORT NUMBER

9. SPONSORING/MONITORING AGENCY NAME(S) AND ADDRESS(ES)

Air Force Research Laboratory
Materials and Manufacturing Directorate
Wright-Patterson Air Force Base, OH 45433-7750
Air Force Materiel Command
United States Air Force

10. SPONSORING/MONITORING AGENCY ACRONYM(S)
AFRL/RXLMN

11. SPONSORING/MONITORING AGENCY REPORT NUMBER(S)
AFRL-RX-WP-TP-2010-4142

12. DISTRIBUTION/AVAILABILITY STATEMENT
Approved for public release; distribution unlimited.

13. SUPPLEMENTARY NOTES

14. ABSTRACT

In this paper, we present results on estimating material model parameters from inverse analysis of full-field deformation data obtained with a prototype of a novel integrated tool consisting of a digital image correlation system and software for data analysis and parameter estimation. Such a tool is needed for characterizing the properties of new materials, and for calibrating and validating material models. The stereo microscope-based image analysis system may be used for measurements at temperatures up to 750°C, and field sizes of approximately 1 mm. The Graphical User Interface (GUI)-based parameter estimation tool integrates image data analysis and inverse analysis modules, and incorporates features for interfacing the tool with commercial finite element (FEM) packages. Data analysis includes filtering or correcting for rigid body translations and rotations, and averaging for noise reduction.

15. SUBJECT TERMS
novel integrated tool , calibrating, validating, Graphical User Interface (GUI)

16. SECURITY CLASSIFICATION OF:			17. LIMITATION OF ABSTRACT:	18. NUMBER OF PAGES	19a. NAME OF RESPONSIBLE PERSON (Monitor)
a. REPORT	**b. ABSTRACT**	**c. THIS PAGE**	SAR	16	Reji John
Unclassified	Unclassified	Unclassified			19b. TELEPHONE NUMBER *(Include Area Code)* N/A

An Integrated Tool for Estimation of Material Model Parameters

S. Ghosal*, N. Acharya, T. E. Abrahamson
SC Solutions, Inc., 1261 Oakmead Pkway, Sunnyvale, CA 94085

H. W. Schreier
Correlated Solutions, Inc.

(*Corresponding author. Email: ghosal@scsolutions.com)

ABSTRACT:

In this paper, we present results on estimating material model parameters from inverse analysis of full-field deformation data obtained with a prototype of a novel integrated tool consisting of a digital image correlation system and software for data analysis and parameter estimation. Such a tool is needed for characterizing the properties of new materials, and for calibrating and validating material models. The stereo microscope-based image analysis system may be used for measurements at temperatures up to 750°C, and field sizes of approximately 1 mm. The Graphical User Interface (GUI)-based parameter estimation tool integrates image data analysis and inverse analysis modules, and incorporates features for interfacing the tool with commercial finite element (FEM) packages. Data analysis includes filtering or correcting for rigid body translations and rotations, and averaging for noise reduction. The GUI, together with a micrograph of the sample, is used to select a subset of the imaged region for analysis, and for specifying sample grain boundaries needed for developing the FEM model. The inverse analysis module runs the FEM simulation under the experimental loading within its iterative loop, using the downhill simplex method for parameter estimation. The methodology was successfully validated from measurements on a superalloy sample.

1   An Integrated Tool for Full-field Measurements and Model Calibration

In recent years, complex multi-scale material models have increasingly been used in design and analysis for various engineering applications. The scope of these physics-based models is varied, dealing with stress-strain relationships, defect initiation and growth, thermal behavior, fracture mechanics, etc. The purpose of attaining predictive capabilities using the material models is to estimate the performance, safety and reliability of the components that are developed using these materials and operate under a wide range of conditions, whether it is for lifetime prediction of existing mechanical components, or for predicting the performance limits of components designed with new, engineered materials. However, for these models to be used reliably, they need to be calibrated and validated.

A formal overall approach was presented by Johnson *et al.* [1] with the goal of efficient model validation. This approach integrates experiments with a software platform where optimization techniques use FEM models of the sample and the data to estimate model parameters. In a typical experiment, the solid sample is subjected to a sequence of step changes in load conditions. A series of images of a sample's region-of-interest (ROI) is acquired at each load step. The images are then precisely aligned and evolution of the displacements is calculated from the difference of each of the images relative to a reference image following extensive image analysis [1]. As shown in Figure 1, an iterative inverse analysis is required in order to estimate the material parameters of the model.

We have developed this concept into a novel integrated measurement, analysis, and parameter estimation

tool that enables materials engineers and researchers to make deformation measurements of materials at high magnification and at high temperatures, then analyze the data, and run parameter estimation calculations using commercial FEM models of the sample in iterative loops within the tool. In this section, we give an overview of the tool; the following sections detail results obtained for a material parameter estimation application
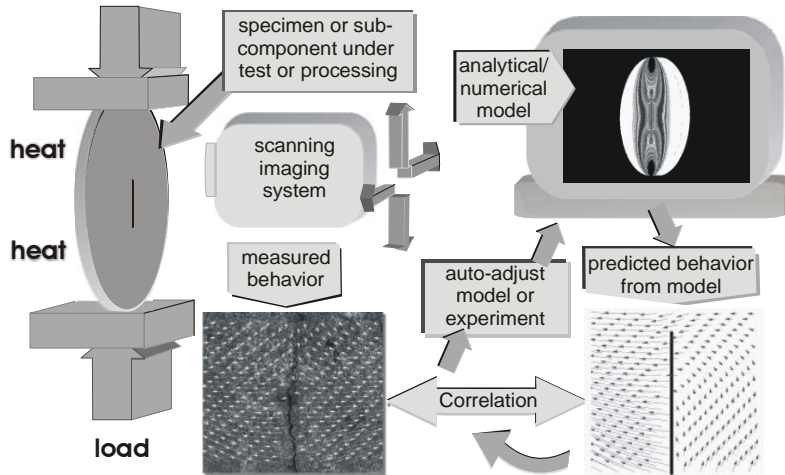

Figure 1: Schematic representing the process material model parameter estimation [1].

We have designed and developed a new high-magnification stereo microscope-based Digital Image Correlation (DIC) system (Vic 3D) that can measure deformation up to temperatures of 750°C with sub-micron resolution. DIC is a non-contacting measurement technique widely used in experimental mechanics to acquire full-field deformation measurements [2]–[6]. The technique uses a random dot pattern applied to the test article to track the deformation on the surface (see Figure 2). During the experiment, images are taken at intervals, and digital image correlation is then used to determine the deformation in the image plane. In order to relate the displacements found in the image plane to object displacements, a calibration, is performed. The calibration permits a three-dimensional reconstruction of the object shape, as well as the determination of the complete, three-dimensional displacement vector field.
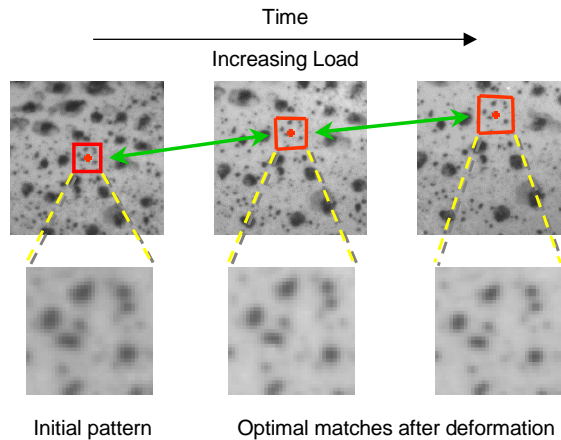

Figure 2: Tracking of object deformation using Digital Image Correlation.

The underlying concept of DIC is the measurement of displacement (and possibly displacement gradients as well as higher-order terms) at a point in an image by considering the gray value pattern in a small neighborhood. Given a second image, the objective of the method is to find the displacements (and possibly higher-order terms) that maximize the similarity between the pattern in the original image neighborhood and a displaced (and possibly deformed) version of the same pattern in the second image. An efficient method to solve this problem is the iterative algorithm proposed originally in [3]. Let θ be a parameter vector that contains the image displacements and possibly higher-order terms. Let f_i denote the gray values in the original image neighborhood, and $g_i(\theta)$

denote the corresponding gray values in the image *after* deformation. An objective function, **E**, is defined and minimized using standard numerical methods to obtain the best parameter estimate, θ.

$$\mathbf{E} = \sum_i \left(f_i - g_i(\theta) \right)^2 .$$

The objective function could be based on the sum of squared differences as shown above, or use the normalized cross-correlation as well as the zero-mean normalized cross-correlation criteria for improved performance. The resolution capabilities of the DIC method have been shown to be better than 0.01 pixels for displacements with negligible bias [5], [6]. Since the digital image correlation method acquires displacement and strain data over the entire specimen area being imaged, it is ideally suited to measure non-homogeneous deformation fields.
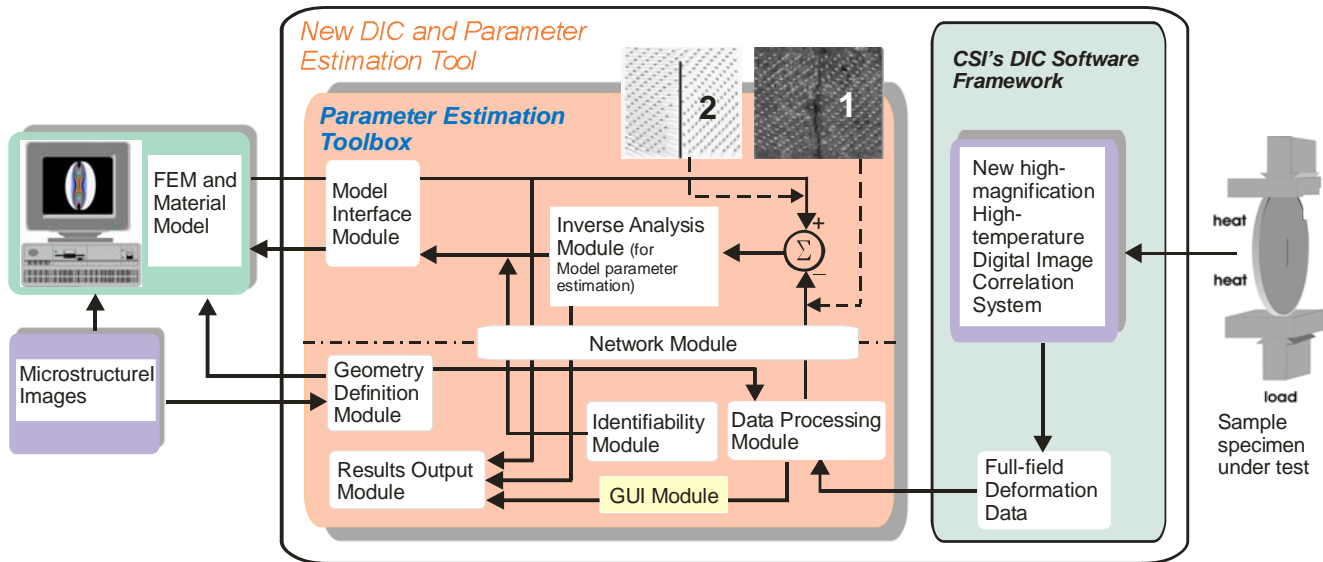

Figure 3: Functional and architectural schematic overview of the tool prototype. The images 1 and 2 show the deformation fields from FEM computations and the DIC data, respectively.

Figure 3 shows a high-level schematic of the tool. The deformation data produced by Vic 3D is an input to the Parameter Estimation Toolbox (PET), which consists of eight functional modules that exchange data (mostly through files) as shown by the arrows in Figure 3:

- The *Model Interface Module* implements a protocol for exchanging data with the user-created FEM model (using third-party software) of the sample that incorporates the material model.
- The *Geometry Definition Module* allows the user to interactively identify the grain boundaries in the form of polygons using a digital image of the microstructure, and also specify regions that the user wishes to exclude from the parameter estimation computations, e.g., because the deformation data is not sufficiently accurate.
- The *Identifiability Module* allows the user to run the FEM model and test the sensitivity of the deformations under the test conditions to the material parameters.
- The *Data Processing Module* performs extensive pre-processing of the data from Vic 3D (including data averaging, transformations, etc.) to allow the user to manage the large amounts of deformation data from Vic 3D.
- The *Inverse Analysis Module* uses optimization algorithms to determine the optimal values of the material model parameters that minimize the difference between the measured and modeled displacements while running the FEM model in an iterative loop.
- The *Results Output Module* incorporates several file manipulation and plotting routines to graphically display results of data analysis and parameter estimation computations.
- The *Graphical User Interface (GUI) Module* serves as the interface to all the other modules, and it ties the various modules together into one user-friendly tool. It will enable the user to develop, control, and examine the results of data processing and the parameter estimation process on a Windows desktop.

- The *Network Module* allows the user to control the process using the GUI Module from the Windows machine while the actual computation may be optionally performed on a different high-performance computer (Windows or Linux). The data and the results being generated are available to the user for interaction and visualization purposes *via* the GUI. The modules and the FEM software (shown above the dot-dashed line in Figure 3) can run on a separate computer while the remaining modules run on the host Windows computer.

The hardware-software tool is innovative in many ways. The high magnification stereo-microscope system permits deformation measurement with sub-micron resolution. The furnace with optical access enables measurements at high temperatures using the stereo microscope. The parameter estimation software has been designed to be modular and can be adapted to various applications relatively easily. For example, the PET can be interfaced with a wide range of commercial FEM packages and various data formats. It can incorporate new optimization techniques, and can use deformation data from multiple sources.

2   Experiment and Data Analysis

As a demonstration of the tool, deformation measurements under tensile loading were performed on a dogbone sample made of single-crystal nickel superalloy. The dogbone dimensions were 50 mm (length), 8 mm (width, 3 mm in the neck region) and 1.5 mm (thickness). The rectangular measurement area of dimension 7.4 mm by 2.8 mm was located at the center of the sample on one surface.

During the experiment chosen for validating the parameter estimation method, 388 image pairs were acquired before specimen failure, resulting in approximately 1.4 GB of image data. The images were processed using Vic-3D, and approximately 60,000 data points per load step were analyzed. The Bunge-Euler angles, Φ_1, Ψ and Φ_2, were used to characterize the orientation of the crystal axis of the single-crystal sample.   Sequential rotations about the laboratory coordinate axes (or the primary axes of the sample) bring the former into alignment with the material axes (or the principal crystallographic directions). The values of these angles were measured separately as $\Phi_1 = 8.6°$, $\Psi = -3.2°$ and $\Phi_2 = -8.3°$.

The raw DIC data was averaged at each FEM mesh point using an exponential weighting function that dropped whose shape is specified by the user of the tool. For this sample, the displacement data at each of the 1071 grid points is an average of between 50–200 raw data points (depending on the measurement locations) for a total of over 60,000 data points. The data was then filtered to remove rigid body translation and rotation using following filter *at each load*:

$$F \ = \ \begin{cases} u + u_0 - u_{left\_edge} \\[2mm] v + v_0 - \text{mean}(v) \\[4mm] \min_{\theta} \left| R(\theta) \begin{bmatrix} u \\ v \end{bmatrix} \right|_{y=0} \end{cases}$$

Here, u_0 and v_0 are the offsets to account for displacement measurements starting at a non-zero load. The third operation is the rotational transformation which corrects the rigid-body rotation. We will refer to the filtered displacement data as u_f, v_f, and w_f. The filtered v profiles are shown in Figure 4.

For the plastic deformation data we found that the filtering could not correct the distortions in the y-displacements because these distortions are not caused by rigid body rotation, but due to the large localized deformation in u_f and w_f near the top right corner. We need to use the v_f data for our parameter estimation. Since the geometry and loading are symmetric in the FEM model, non-symmetric deformations as seen in the data are not predicted. Hence, we chose to use the *change in the width* of the measurement area for our optimization cost function computations instead of v_f. This width change data was still too noisy for use in parameter estimation calculations. To reduce the noise, we computed the best-fit slope of the normalized load, F' *vs.* scaled average change in width of the measurement area, $\delta \overline{v}_o'$, which are defined as:

$$F' = \frac{F - F_1}{F_2 - F_1}; \qquad \delta\overline{v}_o' = \left(\delta\overline{v}'\right)_F - \left(\delta\overline{v}'\right)_{F=F_1}$$

Here, F_1 and F_2 are the loads at the beginning and end of each plastic region. The scaled change in width at any load with the offset, $\left(\delta\overline{v}'\right)_F$, was calculated as:

$$\left(\delta\overline{v}'\right)_F = \frac{(1/n_x)\sum_x\left[\left(v_f\right)_{y=y_{\min}} - \left(v_f\right)_{y=y_{\max}}\right]}{\max\left((1/n_x)\sum_x\left[\left(v_f\right)_{y=y_{\min}} - \left(v_f\right)_{y=y_{\max}}\right]\right)}$$

The scaling ensures that the slope has a magnitude of the order of unity rather than the very large values that would be obtained if the actual loads and changes in widths were used.
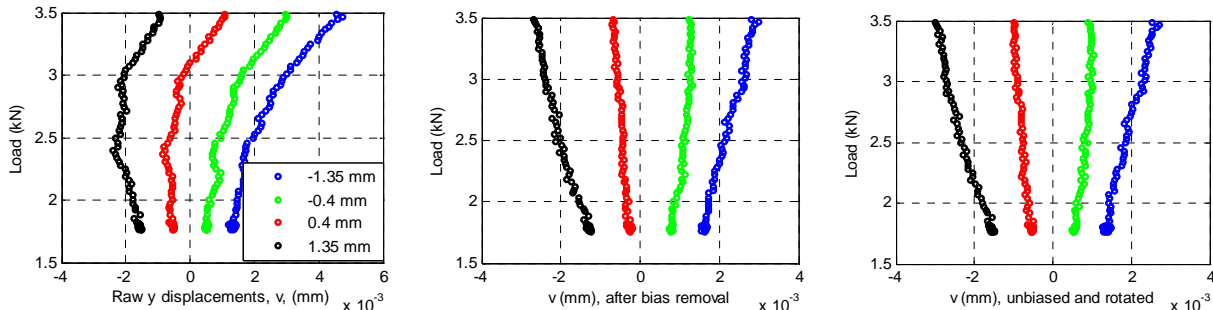

Figure 4: Effect of translation and rotation on load *vs.* elastic *v* data at three points along the vertical centerline of the sample. Left: raw data. Center: data after the mean value of *v* has been subtracted. Right: final filtered data, v_f, after performing rigid body rotation on data from the second figure.

3   Finite Element and Material Models

3.1   Geometry, Mesh, and Boundary Conditions

We developed a 3D FEM model in ADINA®, a commercial software product, for the dogbone sample. The mesh used consisted primarily of quad bricks, and the total number of mesh points was 9894. The measurement area was meshed separately from the rest of the dogbone with a rectangular grid of 51×21 points along the *x* and *y* axes. This separate meshing was performed for convenience to obtain a higher mesh density in the measurement area. One end of the dogbone was fixed (resulting boundary condition: fixed *u*, free *v* and *w*) while the other face had force boundary conditions (equal forces at all the nodes on that face that add up to the total applied force, free *u*). Additionally, *v* and *w* were fixed on the end points of the longitudinal centerline on one surface.

3.2   Elastic Region

The single-crystal superalloy has been modeled as a simply orthotropic material, with stresses and strains in the primary (material) coordinate system given by [7]:

$$\begin{bmatrix} \vec{\sigma} \\ \vec{\tau} \end{bmatrix} = C_{ij}\begin{bmatrix} \vec{\varepsilon} \\ \vec{\gamma} \end{bmatrix}$$

Here, the elasticity stiffness matrix, C is a 6×6 matrix, and for simply orthotropic materials, only 6 out of the 36 elements are independent:: $E_1(=E_2)$, E_3, G_{12}, $G_{23}(=G_{13})$, ν_{12}, $\nu_{23}(=\nu_{13})$.

3.3   Plastic Region

The non-linear plastic region was modeled using Hill's model for yield and a multilinear hardening rule as described in this section. We assume that the sample does not undergo creep, *i.e.*, that the strains are only dependent on the load and are time-independent at a given load.

The Hill's yield model has six parameters which are the yield stresses in the directions of the material axes (*1, 2, 3*) and the yield stresses for pure shear in the material planes (*12, 23, 13*), i.e., $\sigma_{Y,1}$, $\sigma_{Y,,2}$, $\sigma_{Y,,3}$, $\sigma_{Y,12}$, $\sigma_{Y,23}$, $\sigma_{Y,13}$, respectively. We use a single universal plasticity modulus, E_p^u for modeling hardening [8]. Effective Poisson ratios along the material axes (denoted by subscripts 1, 2, and 3) are used, and these are related *via* a Lankford coefficient and volume conservation as shown in the equations below.

The Lankford coefficients were originally defined for rolled plates [9]. Typically, three specimens are cut from a rolled plate, with angles of 0º, 45º, and 90º to the rolling direction (direction '*a*'). The ratio of the plastic strain in the specimen direction transverse to '*a*' (direction '*b*') to the through-thickness (direction '*c*') plastic strain is the Lankford coefficient. In ADINA's implementation of this plasticity model, there are five independent parameters: $\sigma_{Y,1}$, r_0, r_{45}, r_{90}, and E_u^p.

The elasticity and plasticity models used would treat the single-crystal superalloy as a bilinear system. The plastic region, however, is non-linear. To accommodate the non-linearity, we divided the non-linear region into three piecewise-linear regions, as shown in Figure 5, which plots load *vs. u* that was measured on the single-crystal sample at the center of the measurement region. The three locally-linear regions are marked Plastic1, Plastic 2 and Plastic3, with end-points corresponding to loads of 3.68 kN, 3.72 kN, and 3.75 kN, respectively. The deformation continues to increase with small increases in load, and additional locally linear regions can be identified. However, for purposes of demonstration of the parameter estimation technique, we will restrict ourselves to three zones. Hence, a set of Lankford coefficients is needed for each of the three linear segments that approximate the plastic region. Of course, the relationship to yield stresses *via* the Hill parameters is meaningful only for the first linear plastic zone.
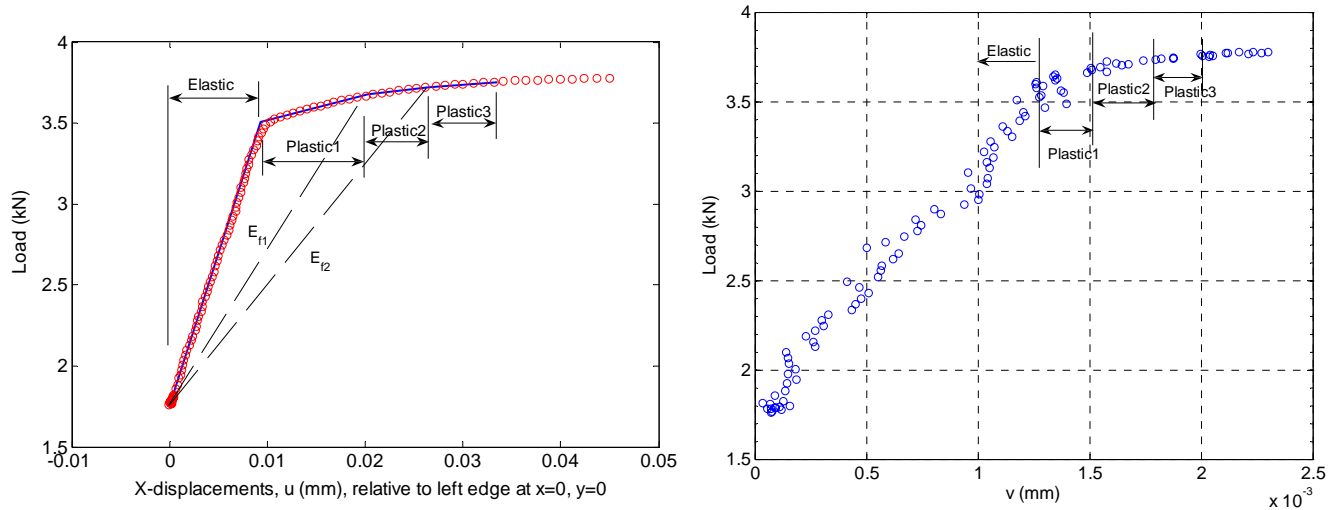

Figure 5 : Left: Load *vs. u* data at the center of the measurement region for the single-crystal sample. Right: Load vs. *v* data at x = 0, y = -1.35 mm for the single-crystal sample.

4 Model Parameter Estimation for the Elastic Region

The generalized cost function, *J*, used for parameter estimation is computed as the two-norm of the normalized error between the model prediction and the experimental values of *Y*, averaged over the total number of measurement axes (*n*) and FEM models (*m*). Here *Y* represents either the (filtered) measured displacements, or the best-fit slope of the load *vs.* displacement graph:

$$ J \;=\; \frac{1}{m}\sum_{i=1}^{m}\left[\frac{1}{n}\sum_{j=1}^{n}\left\{\sqrt{\frac{1}{N}\sum_{k=1}^{N}W_{i,j,k}\left\|\frac{Y_{E,i,j,k}-Y_{M,i,j,k}}{Y_{E,i,j,k}}\right\|^{2}}\right\}_{j}\right]_{i} $$

The subscripts *E* and *M* refer to the experimental data and model results, respectively. The number of good data points (i.e., mesh points where the displacement measurements are sufficiently accurate) in the ith model along the jth axis is $N_{i,j}$. Since we are using only one FEM models, *m* = 1. Also, since we are not using *w* data, *n* = 2. Each data point has a weight $W_{i,j,k}$ that can have any value between 0 and 1.

After performing sensitivity calculations for parameter identifiability, it was found that only two of the six parameters in this orthotropic model showed sensitivity to the measured displacements, and hence only these two (E_1= E_3, E_2) could be estimated. The reason for this limitation is two-fold. First, the out-of-pane *w* data was too noisy to be useful. Second, for small values of Bunge-Euler angles, σ_2 and σ_3 are non-zero in the material coordinate system but of very small magnitude. Consequently, the dependence of *u* and *v* on material

parameters other than E_1 and ν_{12} (through elements of C_{ij}) is very weak. If the material axes are substantially out of alignment with the global coordinate axes, the stress vector will be full, and thus the displacements measured (or equivalently, the cost function for parameter estimation) would have significant sensitivity to all the material parameters.

Inverse analysis was performed using the downhill simplex method, a robust search algorithm that has been successful in finding the global minimum of various non-linear cost functions [10]. Table 1 shows the values of the Young modulus along the (*1, 2*) material axes starting from two different sets of trial values that are quite far apart. Figure 6 shows the load *vs.* displacement (v_f) graphs from the FEM model using these optimal parameters and with the data. Good agreement between the model and data is seen in the elastic stage. For the other four parameters, we use nominal values for this material of $\nu_{12} = \nu_{13} = 0.38$, $\nu_{23} = 0.3$, $G_{12} = G_{13} = 100$ GPa, $G_{23} = 110$ GPa. The values of E_1 and E_2 obtained here compares well with the effective modulus of 138.3 GPa in the loading direction calculated from the gross measurements. On a Linux workstation powered by an AMD Opteron 248 running at 2.2 GHz with 12 GB of RAM machine, the optimization computations took approximately half an hour to converge (Figure 7). Almost all of the time is used for the cost function computations, i.e., running the ADINA[®] simulations.

Table 1: Optimal parameters (elasticity model) for the single-crystal sample.

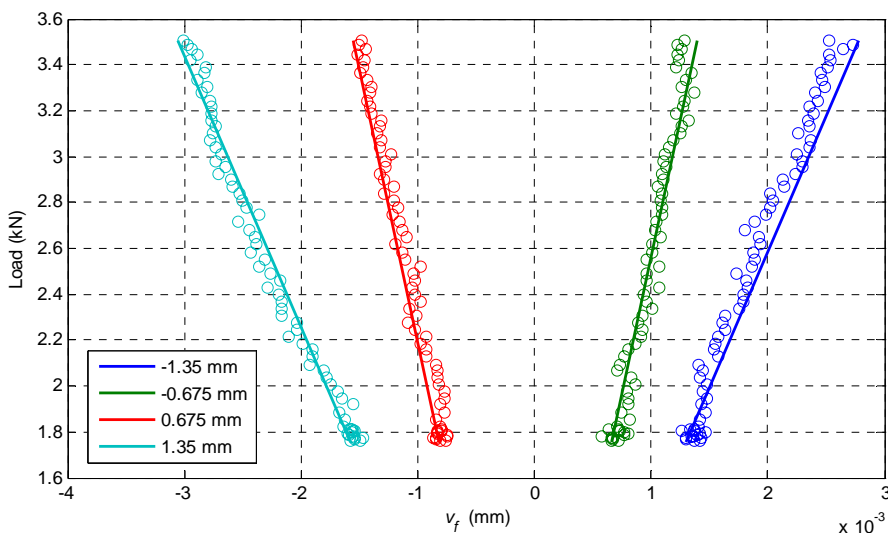|	Run 1		Run 2	
	Initial	**Final**	**Initial**	**Final**
E_1 **(GPa)**	80.0	129.5	180.0	129.5
E_2 **(GPa)**	80.0	141.6	180.0	141.6

Figure 6: Load *vs.* v_f at four points along centerline (*y*=0). in the elastic regime. Circles are experimental data and the straight lines are FEM model results for optimal material parameters
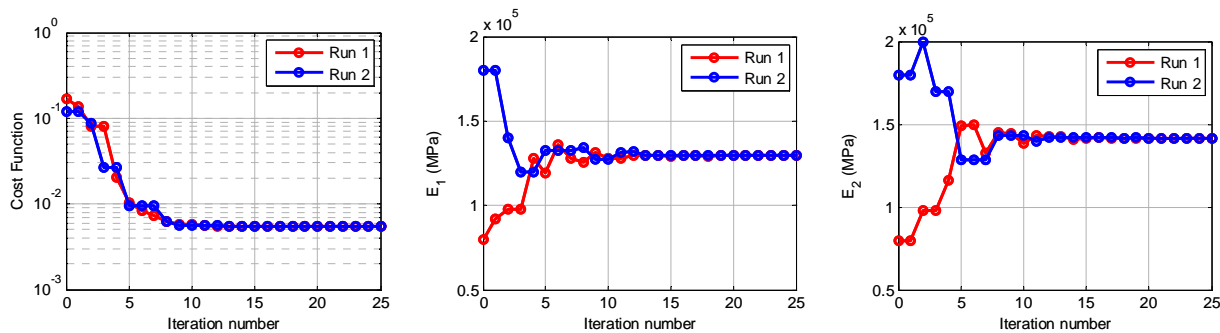

Figure 7: Convergence plots for the estimated material parameters of the single crystal sample, and the associated cost function..

5   Parameter Estimation for the Plastic Region

As stated earlier, we have modeled the plastic region as consisting of three piece-wise linear segments (marked Plastic1, Plastic2 and Plastic3 in Figure 5), each with its own universal plasticity modulus and Lankford coefficients. We first estimate the parameters for Plastic1 zone. The elastic properties are specified as the values determined from the elastic analysis of Section 4. In order to implement the model for plastic zones 2 and 3, we assume that the boundary point between zone 1 and 2 is the yield point of a fictitious material with elastic properties E_{f2}, as shown using dotted lines in Figure 5. Next, we estimate the elastic properties of this fictitious material, and the plastic properties (yield stresses, universal plasticity modulus and Lankford coefficients). We discard the elastic properties and the yield stresses and retain the Lankford coefficients and the universal plasticity modulus for the zone Plastic2. This procedure is then repeated for the third plastic zone.

Sensitivity analyses showed that for this single crystal sample under the imposed loading condition, we can estimate only three of the five parameters: $\sigma_{Y,1}$, r_0, and the universal plasticity modulus, E^u_p. The other two coefficients are assigned the following values: $r_{45} = 0.2$ and $r_{90} = 0.05$. These approximate values were determined from the measured strain ratios in the three directions. The plasticity model involves both the yield stress and hardening behavior model parameters (Lankford coefficients). Consequently, in our linearized (slope-based) approach to the plastic zone, we have to tie down the plasticity slope to the yield point. To this end, the cost function was modified to incorporate the error in the displacements at the yield load. The cost function, J, was re-defined for plastic zone 1 as:

$$J = \frac{\sum_{j=1}^{2}\sum_{k=1}^{N}\left\|\frac{Y_{E,j,k} - Y_{M,j,k}}{Y_{E,j,k}}\right\|^2 + 0.25*\sum_{k=1}^{N}\left\|\frac{u_{f,E,k} - u_{f,M,k}}{u_{f,E,k}}\right\|^2}{2N}$$

Here u_f is the filtered x-displacement at yield load. This term was weighted by 0.25 to reduce the potential effect of noise in the u data on the optimization accuracy. The choice of the factor of 0.25 was reached after trying a few other values for fastest convergence. Y is the best-fit slope to the load-displacement plot. The subscripts j refers to the axis (x or y), k represents the data point number, and E and M refer to experimental data and model results, respectively. The optimization computations took approximately 12 hours to converge for Plastic 1 zone, and 6-7 hours for the other two plastic zones on the AMD Opteron workstation running at 2.2 GHz with 12 GB of RAM.

The optimal parameters for the three plastic zones are shown in Table 2 and Table 3. Figure 8 shows the comparison of the model and data over the entire load range over which parameter estimation had been carried out. The figure on the left shows graphs of average stress *vs.* strain at a single point (center of the sample). The quality of the model fit can be examined more closely in the graphs on the right side of Figure 8 where u_f has been plotted individually for the elastic and the three plastic zones. The fits are very good overall, and the optimization convergence is excellent.

Table 2: Initial and final parameter values for the first plastic zone.

	Run 1		Run 2	
	Initial	Final	Initial	Final
E^u_p (GPa)	10.0	13.7	18.0	13.7
$\sigma_{Y,1}$ (GPa)	0.40	0.77	0.80	0.77
r_o	0.2	0.016	0.025	0.016

Table 3: Initial and final parameter values for the second and third plastic zones.

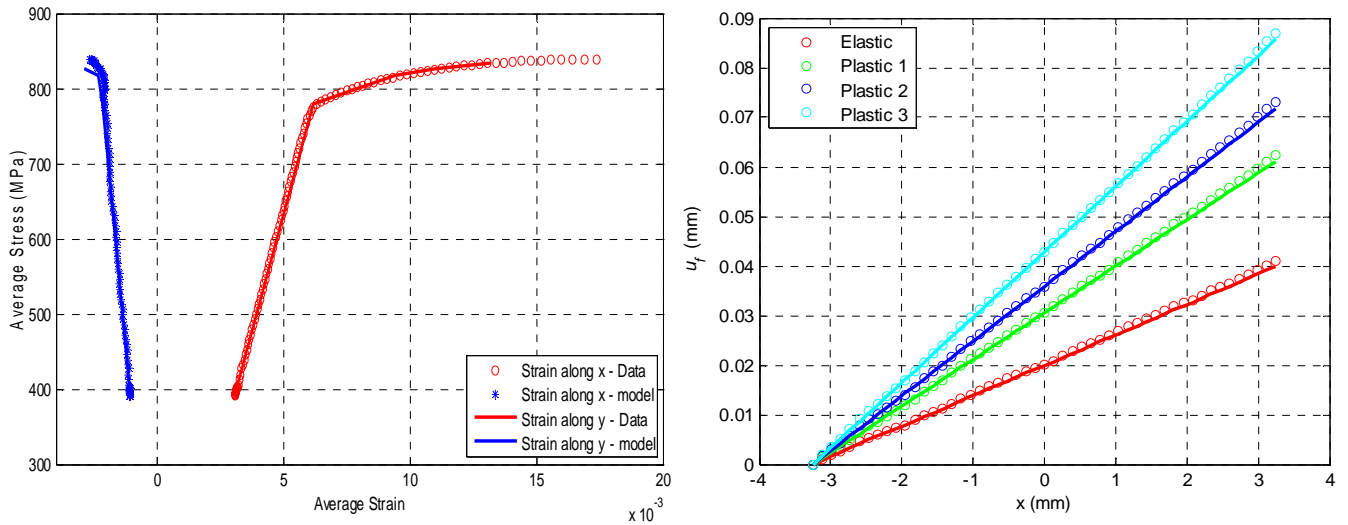|	Plastic Zone 2				Plastic Zone 3			
	Run 1		Run 2		Run 1		Run 2	
	Initial	Final	Initial	Final	Initial	Final	Initial	Final
E^u_p (GPa)	10.0	6.4	5.0	6.4	7.5	3.7	5.0	3.7
r_o	0.05	0.068	0.1	0.068	0.25	0.092	0.1	0.092

Figure 8: Left: Graphs of average stress *vs.* strain in *x* and *y* directions at various *x* points along centerline (*y*=0). Circles are experimental data and the straight lines are FEM model results for optimal material parameters. Right: u_f at all points along the x direction for elastic and plastic regions with displacements in each zone shifted to pass through same starting point.

6   Conclusion

We have demonstrated the capability of a new hardware-software tool to measure full-field deformation data and then process the data for use in estimating the sample's material model parameters. The stereo microscope-based DIC system can handle field sizes of about 1 mm and high temperatures up to 750°C. Measurements were made on a single-crystal nickel superalloy sample. The parameter estimation toolbox processed the vast amounts of DIC data that was generated, and interface with ADINA, a commercial FEM software to run the model in an iterative loop during optimization calculations. The elastic and plastic model parameters converged to the same values which are typical of this material. It was noted that the choice of sample and the quality of the data can have a major impact on the parameter estimation results.

Acknowledgement

References

[1]   D. A. Johnson, W. J. Porter III, R. John, "Full-Field Techniques in the Study of Multi-Scale Nonlinear Material Behavior," Proc. SEM Annual Conference, *Experimentation and Modeling at the Nanoscale*, Society for Experimental Mechanics, Charlotte, NC, 2−4 June 2003.

[2]   T. C. Chu, W. F. Ranson, M. A. Sutton, W. H. Peters, "Application of Digital Image Correlation Techniques to Experimental Mechanics," *Experimental Mechanics*, 25 (3), pp 232 - 245 (1985).

[3]   M. A. Sutton, M. Cheng, W. H. Peters, Y. J. Chao, and S. R. McNeill, "Application of an Optimized Digital Correlation Method to Planar Deformation Analysis," *Image and Vision Computing*, 4 (3), pp 143-150, 1986.

[4]   J. D. Helm, S. R. McNeill, M. A. Sutton, "Improved 3-D Image Correlation for Surface Displacement Measurement," *Optical Engineering* 35:7, pp. 1911-1920, 1996.

[5]   H. W. Schreier, J. R., Braasch, M. A., Sutton, "Systematic Errors in Digital Image Correlation Caused by Intensity Interpolation," *Opt. Eng.*, 39(11), 2000.

[6]   H. W. Schreier, M. A., Sutton, "Systematic Errors in Digital Image Correlation Due to Undermatched Subset Shape Functions," *Experimental Mechanics*, 43(2), 2002.

[7]   R. M. Jones, *Mechanics of Composite Materials*, 2nd Edition, Taylor and Francis, 1999.

[8]   ADINA R&D, *ADINA Theory and Modeling Guide, Volume 1: ADINA Structures and Solids*, p. 278, October 2005.

[9]   W. T. Lankford, S. C. Snyder, J. A. Bausher, *Trans. ASM*, 42:1197, 1950.

[10]   W. H. Press, B. P. Flannery, S. A. Teukolsky, W. T. Vetterling, *Numerical Recipes in C, The Art of Scientific Computing*, Cambridge University Press, Second Ed., 1992.